Influence of primary and secondary air supply on gaseous emissions from a small-scale staged solid biomass fuel combustor

Thomas Kirch,[*,†,‡] Cristian H. Birzer,[†,‡] Philip J. van Eyk,[¶,‡] and Paul R. Medwell[†,‡]

†*School of Mechanical Engineering, The University of Adelaide, Australia*

‡*Humanitarian and Development Solutions Initiative, The University of Adelaide, Australia*

¶*School of Chemical Engineering, The University of Adelaide, Australia*

E-mail: thomas.kirch@adelaide.edu.au

Abstract

The emissions from traditional biomass combustion systems for cooking and heating are, globally, the main cause for premature mortality due to air pollution. A staged combustion process, that separates the thermochemical conversion of the solid fuel and the combustion of the released products, offers potential to reduce harmful emissions for solid fuel combustion and could therefore help mitigate the issue. In the present study, the fundamental combustion behaviour of a small-scale staged combustor was investigated with a focus on an independent systematic analysis of relevant parameters. Natural and forced draft conditions as well as a combination of both was tested. The relative location of primary to secondary air was also varied. When lighting the fuel, higher airflows lead to faster ignition and lower emissions. A steady-state combustion phase is achieved when gasification products are burned

with secondary air, which occurs mainly while the solid fuel is being pyrolysed. After the steady-state phase, char remains as the solid pyrolysis product. Gasification of the remaining char was found to release great amounts of CO, which are emitted from the combustor, in the case of natural draft secondary air (SA). With higher air flows of forced SA, an exceptionally high nominal combustion efficiency (NCE = $X_{CO_2}/(X_{CO}+X_{CO_2})$) can be achieved in the steady-state phase. Forced SA flows cause a longer duration of the steady-state phase from the combustion of raw biomass gasification products into the combustion of char gasification products. This extension leads to a significant reduction of emissions of incomplete combustion. Additionally smaller distances between the SA inlet and the fuel stack, caused lower emissions of incomplete combustion. The combination of forced draft primary air and natural draft SA presented worse combustor performance than under natural draft conditions.

1 Introduction

Approximately 2.8 billion people currently rely on solid biomass fuel to satisfy their cooking and heating needs.[1] Globally, emissions caused by the use of traditional open fires or simple cookstoves are the main cause of premature mortality due to air pollution.[2] This includes 2.89 million and 2.93 million premature deaths annually related to household air pollution from solid fuels and ambient particulate matter pollution, respectively.[3] These findings illustrate the need for clean-burning cooking devices. A reduction of the amount of pollutant emissions released from incomplete combustion through traditional cooking methods could not only lead to health improvements, but also to social as well as environmental benefits.[4,5]

Staged combustors have demonstrated promising results as cookstoves in laboratory studies, compared with other cookstoves. This type of combustor has been shown to produce low emissions of incomplete combustion, carbon monoxide (CO) and particulate matter (PM), in cooking applications.[6,7] Other emissions, such as nitric oxides (NO_x), can also be reduced through staged combustion .[8] The main feature which sets them apart from other types of combustors is the use of pyrolysis and gasification to transform the batch-fed solid biomass fuel into combustible gases, which are subsequently burned separately in time and location.[9] The measurement of gaseous combustion products can provide valuable information to gain a better understanding of the ongoing processes.

The two-staged combustion process is initiated by lighting the fuel from the top with the aid of a kindling material. Lighting has been identified as a major source of emissions of incomplete combustion where the higher heating value of the kindling material and also the supply of forced air can be beneficial .[10] Lighting causes the combustion of the top layer of solid biomass and consumes the oxygen in the combustor, creating a vitiated environment leading to a so-called "migrating pyrolysis front" to establish in which only partial oxidation occurs. This front moves opposite to the primary air (PA) flow, down the fuel stack. Simultaneously, the pyrolysis products are burned separately at a secondary

air (SA) inlet .[11] This separation of pyrolysis and combustion processes is illustrated in Figure 1. The remaining char, which accounts for 20-30% of the initial mass[12–14], can subsequently be burned or used for other purposes such as soil amendment.[15] Three successive processes are most prominent in staged biomass combustors: lighting of kindling material at the top of the fuel stack; the migrating pyrolysis where the release and combustion of volatile compounds prevails; and the char gasification, where the remaining char is converted into CO and CO_2 through surface oxidation. A systematic analysis of each of these phases could aid in decoupling processes to analyse individual parameters in isolation.

The migrating pyrolysis front propagation, and thus the fuel conversion as well as the heat release are controlled by the supply of PA.[12,16–23] It has been shown that forced air can lead to a reduction of emissions of incomplete combustion.[24–26] Conversely, in some cases it is possible that forced air staged combustion stoves, though energy efficient, may not necessarily reduce emissions.[27] These contradictory findings reinforce the need for a deeper understanding of the underlying processes to ensure emission efficiency of future stove designs.

There is widespread belief that forced air, compared to natural draft, leads to greater mixing and thus increased performance.[28,29] Many forced draft stoves are equipped with one single fan that supplies air to both the PA and the SA inlets. The ratio of PA to SA is then fixed, dependent on the stove geometry.[11] However, a few studies have been concerned with the influence of PA[28,30–32] or the ratio of PA to SA[28,29,31,32] on the combustion properties of the combustor. There is a paucity of scientific understanding of such systems and the parameters that control the emissions. In particular, the influence of secondary air flows as well as the relative location to the primary air flow is poorly understood in small-scale staged combustion systems. In continuously-fed domestic biomass boilers iterative parametric investigation of staged air supply has been found to provide means to decrease specific emissions[8,33,34] and could provide similar benefits for the studied com-

bustion system.

The present parametric study was carried out in a research combustor to study and gain a deeper understanding of the ongoing fundamental processes in small-scale staged combustion devices. Preliminary tests under natural draft conditions set a baseline against which alterations can be compared. Subsequently a combination of forced PA and natural draft SA are tested. Since the required air supply will change throughout the different combustion phases it might be advantageous to entrain the SA via natural draft. Further tests are conducted with a specified PA flow and variable SA flow, to study the influence of an increasing air flow on the emissions of the combustion process. The relative location of the SA inlet to the fuel stack is also considered. With a fixed location of the SA inlet a varying distance of the air supply to the fuel might have an influence on the stove performance.

In most research on cooking devices that use biomass fuel, the overall stove efficiency is determined through tests that emulate user practices. This approach is dependent on a multitude of variables, including the combustion and heat transfer properties as well as handling by the user which has been shown to lead to high variability of results.[35,36] This paper focusses solely on the fundamental combustion properties of a small-scale staged combustor, enabling a more independent analysis of relevant parameters. Specifically, the focus of the current work is on the role of the PA and SA supply, and their locations relative to the fuel bed. A deeper understanding of the underlying combustion properties could enable future optimisation of such devices, which is the motivation of this research.

2 Experimental Details

2.1 The Staged Combustor

The research combustor used in the current work has previously been presented[32,37] and shown in Figure2. It incorporates the principal features of a PA inlet at the bottom of

the combustor, and a lateral SA inlet in the upper region. Its dimensions, were chosen to be slightly larger than many commercial products (e.g. the Champion TLUD[11]), especially the height. This increased size enables an investigation of scaling effects over a wider range of combustion-relevant parameters, such as the fuel grate location. Importantly, the large diameter of the vessel provides a nearly one-dimensional reactor to facilitate subsequent modelling. The research combustor has been designed to advance the fundamental-level understanding and to study the underlying physical processes. Thus the combustor will be used to assess the combustion properties, not the cooking performance. It is important to recognise that the current system does not include a pot on top of the stove. If the secondary flame front were to interact with such a pot, localised quenching could occur and subsequently lead to an increase in the emission of the products of incomplete combustion. However, with proper design and operation of a stove, such effects would ideally not occur in an operational stove.

The steel cylinder combustor body has a diameter of 206 mm, a height of 600 mm and a wall thickness of 8 mm. Inside the combustor body the fuel grate, on which the fuel is placed, is held via three hooks. These are attached to the rim of the combustor body: the fuel grate location is variable by adjusting the length of these hooks between 50 mm and 570 mm below the SA inlet. The hooks enable the grate to be easily removable from the combustor for post-combustion analysis of the solid residual matter, as well as for cleaning. The grate is perforated with 3-mm-diameter holes, with an open-area ratio of 26%, which allows PA from beneath the grate to enter the fuel-stack. The combustor body is placed on top of the PA inlet chamber.

2.1.1 Primary Air Configurations

The PA inlet chamber (dimensions: 248 mm $\times$ 248 mm $\times$ 150 mm) is equipped with removable side walls. When the side walls are taken off, the air can enter freely over the whole combustor body diameter via natural draft, and if closed off, air can be applied

through a controlled inlet. In the natural draft configuration, the amount of air that enters is determined by the buoyancy force due to the pressure difference over the combustor height during the combustion process. In the forced air configuration, the sides of the chamber are closed off and the inlet is connected to dry compressed air. The in-flow is controlled by a needle valve and a rotameter upstream of the inlet. Downstream of the inlet, air passes through a diffuser ring with ten 1-mm-diameter holes. These holes in the diffuser are directed downward which forces the air flow to be inverted before entering the combustor body. The inversion of the PA flow leads to less swirl and a more uniform airflow through the combustor body. Subsequently the flow through the combustor body is influenced by the porous fuel bed. The air flow through direction in the combustor is presented in Figure 2. In the present study, tests were performed in the natural draft as well as the forced air configuration.

2.1.2 Secondary Air Configurations

The SA enters the combustor through three 190-mm long, 20-mm high, lateral openings. These are located 285 mm below the top of the combustor extension, and 55 mm above the exit plane of the combustor body. There are two different configurations which allow air to enter either via natural draft or forced by introducing compressed air. For the natural draft configuration, the three openings of the combustor extension, shown in Figure 2, are open to the surroundings. In the forced air configuration, the inlet is enclosed by a diffuser skirt. The forced air combustor extension has four inlets. All four inlets are connected by hoses of equal length to a manifold. The manifold is situated downstream of a needle valve and rotameter by which the inflow of dried compressed air is regulated. These measures were taken to ensure a uniform flow throughout the skirt to enter the combustor extension. In all forced air configurations PA and SA are separately controlled via independent air supply lines.

2.2 Data Collection

The data collection set-up consists of emissions data being collected in one central location while temperature data was constantly measured in two locations. The research combustor was placed under a fume hood, which was connected to an extraction duct and a fan to ensure that all emissions from the combustor were directed outside of the laboratory. The measuring probe of a Testo 350XL gas analyser was placed 830 mm above the exit plane, along the central axis of the research combustor. This sampling location is at the interface of the fume hood and the extraction duct. The released gases from the research combustor will expand upon leaving the combustor, mix with the surrounding air and enter into the fume hood. The hood acts as an aerodynamic contraction, reducing the 1060-mm intake down to a diameter of 185 mm at the point the measurements are collected. The diameter of the fume hood intake compared with the research combustor diameter ensures that all emissions from the reactor are collected. The high contraction ratio of the fume hood promotes intense mixing of the gases, such that the emissions from the combustor are well-mixed by the time they reach the measurement point. The gas analyser was used to measure the CO, CO_2 and H_2 emissions at 1 Hz, on a dry basis. The resolution was 1 ppm for low emission levels ($<$2000 ppm and 5 ppm for high emission levels ($>$2000 ppm) of CO measurements. The resolution for CO_2 measurements was 0.01%. For all measurements, unburned hydrocarbons (methane, propane and butane) were below the detection limit, namely 100 ppm. Temperature data were collected, at 1 Hz, via two K-type thermocouples inside the combustor body and the combustor extension, shown in Figure 2 at locations A and B, respectively. For procedural purposes temperatures were measured in location C, when needed, via an infra-red thermometer.

2.3 Test Procedure

The research combustor, with a wall thickness of 8 mm, has a higher thermal mass than usual cookstoves. It therefore was deemed necessary to ensure that only pre-heated tests were recorded, to minimise any influence on the combustion performance, although the process can also be achieved with a cold start. After pre-heating the combustor a new batch of fuel was introduced when the outer wall temperature in location C, shown in Figure 2, measured 150° C. For kindling, 5 mL of methylated spirits (96% ethanol, CAS # 67-63-0) was poured over the fuel stack and ignited when the outer wall temperature reached 135°C. The chosen starting wall temperature of 135°C is below the temperature encountered later in the burn-cycle. Therefore, thermal energy from the combustion goes toward increasing the body temperature. However, it is not possible to preheat to a higher temperature both for manual handling safety during the reload process, and also to avoid volatilisation of the biomass fuel, which starts at approximately 200°C.[26]

The fuel for each test consisted of 700 g of dried locally sourced pine chips (*Pinus radiata*). The wood chips were obtained from various locations across the Mt Lofty ranges of South Australia. They were sourced in-bulk, as pre-chipped material, and sieved through a 25 mm aperture, resulting in an average particle size of 24 mm $\times$ 8 mm $\times$ 3 mm (length $\times$ width $\times$ height). The bulk density of the dried pine chips is approximately 210 $kg \cdot m^{-3}$. This density and amount of fuel used led to a fuel bed height of 100 mm and a test duration of approximately 600 s. While a greater amount of fuel would extend the time spend in the steady-state and char phase, it would not impact the findings. The proximate analysis of the pine chips provided a composition of 16.8 % fixed carbon, 82.9 % volatile matter and 0.4 % ash, mass fraction on dry basis. The ultimate analysis yielded mass fractions of 51.2 % C, 6.2 % H, 42.0 % O and 0.2 % N, on a dry basis. Pine chips were chosen as fuel because wood is the most commonly combusted biomass.[38] The influence of the moisture content has previously been studied[13] and is outside the scope of the presented research study. To avoid the influence of inconsistent moisture content on the burning rate and the

emissions,[13] all the chips were dried prior to testing. This was done by keeping them for 16 hours in a confined space at a constant temperature of 37°C, created by an air conditioning unit. The drying process resulted in a fuel moisture content of approximately 7 % determined via the American Society for Testing and Materials (ASTM) D4442-92(2003) standard procedure.[39]

Four sets of tests were conducted with various different configurations presented in Table 1. The first set of tests are performed with both the PA and SA inlet in natural draft configuration. These natural draft tests can be considered as a baseline against which the various alterations of PA and SA flow can be compared. The following sections provide details about the respective variations within each set of tests.

2.3.1 Primary Air Testing

The PA flow is varied while SA is introduced through natural draft. The PA flow rates are 78, 98, 118 and 138 $L \cdot min^{-1}$, corresponding to 47.0, 59.0, 71.0 and 83.2 $g \cdot m^{-2} \cdot s^{-1}$ respectively. The flow rates are reported at STP conditions, namely 0°C and 10^5 Pa. These values were chosen in accordance with previous studies on fixed bed reactors and provide an oxygen-limited environment for the migrating pyrolysis.[16–18,20,21] They are also similar to values and extending the range of a previous study on a similar combustor.[30]

2.3.2 Secondary Air Testing

For the SA tests, the PA flow was set to a value of 118 $L \cdot min^{-1}$, while SA flows of 328, 410, 492, and 574 $L \cdot min^{-1}$ were injected into the combustor extension. No previous studies have been found in which specified flowrates of SA were introduced into a staged combustor. Therefore, an approximation was performed based on previous findings. It has been reported that during the migrating pyrolysis the primary air to fuel (A/F) mass ratio settles at about 1.5 for different PA flow rates.[30] From the ultimate analysis a mole fraction of $C_{1.00}H_{1.45}O_{0.62}$ can be derived for the pine chips, with a respective stoichiometric A/F

mass ratio of 6.2 for complete combustion. Assuming an A/F mass ratio of 1.5 during the migrating pyrolysis[30] the overall fuel equivalence ratio (ϕ) would be 1.11, 0.94, 0.81 and 0.71, for the different SA air flows respectively. Therefore, fuel-rich conditions can be expected for the 328 L·min^{-1} case but fuel-lean conditions for all other flow rates.

2.3.3 Varying Fuel Grate Location Testing

The location of the fuel stack within the combustor was varied to change the residence time of the gases within the combustor body. The tests were performed with the fuel grate at a distance of 180 mm, 270 mm, 370 mm and 470 mm below the SA inlet, as presented in Figure 2. The PA flow was set to a constant value 118 L·min^{-1} and the natural draft combustor extension was attached to the combustor body.

2.4 Data Processing

To account for dilution and determine a quantitative value for the combustor efficiency, the measured emissions were normalised. This normalisation was performed by relating the measured concentrations to all gaseous carbonaceous combustion products. This include the calculation of the nominal combustion efficiency (NCE = $X_{CO_2}/(X_{CO}+X_{CO_2})$ where X is mole fraction), which has previously been established for the evaluation of cookstoves.[40] The only gaseous carbonaceous species that were considered in the normalisation were CO and CO_2, as the hydrocarbon emissions were below the detection limit.

The three expected phases of operation are (1) the lighting phase, (2) the steady-state phase and (3) the char phase. Rigorous analysis identified that all three phases could be identified based on the transition between phases. A mathematical decision rule was used to separate the three phases, to be able to analyse each phase separately. When the temporal derivative of the normalised CO profile exceeded a value of ± 0.002 s^{-1} a change in phase was identified. This value was established to be a robust identifier of a change

in phase. Figure 3 presents an example emissions profile, divided into the three phases by the mathematical decision rule. For each of the three phases, peak values or time-weighted-average (TWA) values were calculated. In the lighting phase the average of the peak values, over all repeat runs, were calculated because this measure is best suited to the transient processes where peaks occur. For the steady-state phase TWA values provide an average value for the steady emissions. For the char phase, both average peak values and TWA values were calculated to account for multiple emissions peaks experienced in this phase.

3 Results

3.1 Natural Draft

Preliminary tests were conducted with the research combustor in its natural draft configuration. The results from these natural draft conditions are presented within the figures of the results from the other sets of tests such that the natural draft case serves as a reference point. In this way, it is possible to see if changing operating parameters can enhance the performance and mitigate emissions of incomplete combustion.

The natural draft tests were used to identify the different combustion phases, the lighting phase, the steady-state phase and the char phase (as previously described in detail[41]). In the lighting phase the kindling material is lit on top of the fuel stack leading to the combustion of the top layer of the solid biomass fuel. In this phase, high emissions of incomplete combustion, namely CO and H_2, were detected, as can be seen in Figure 4. In the steady-state phase the nominal combustion efficiency (NCE) is very high, accompanied by low emission of products of incomplete combustion. In the char phase the NCE decreases significantly and the emissions of CO rise.

3.2 Variation of Primary Air

The emissions and gas-phase temperature profiles with varying PA flows and natural draft SA flow are presented in Figure 4. As explained previously, the three combustion processes of lighting in the first 76 to 102 s, the steady-state combustion in the following 178 to 281 s and after that the char gasification were identified. For the measured emissions, average peak values were calculated for the lighting phase and time weight average values were calculated for the steady-state as well as the char phase, as presented in Table 2.

It can be seen in Figure 4 that in the lighting phase the normalised peak NCE and the measured gas-phase temperature inside the combustor body rise while the normalised H_2 emissions subside substantially with an increase in PA flow. This is consistent with a previous study,[10] which also showed that higher air flows lead to a higher rate of combustion. In the natural draft case, the emissions of products of incomplete combustion are much higher than those in all the forced air cases, except the 78 $L \cdot min^{-1}$ case. To start the process the fuel is placed inside the combustor body and lit from the top. The initial combustion of kindling material and the top layer of biomass consumes the surrounding oxygen inside the combustor body. In the forced draft cases the airflow through the fuel bed provides the necessary oxygen for further combustion, while in the natural draft case the flow has to be established by the buoyancy force. Thus to start a flow through the fuel stack the buoyancy force has to exceed the pressure drop imposed by the fuel stack. This pressure drop could lead to a lower PA flow in the beginning causing the high emissions in the lighting phase. A comparison of the natural draft and varying primary air test results suggest that the average natural draft flow rate is close to 98 $L \cdot min^{-1}$.

Increasing the PA leads to a higher fuel conversion and a shorter time in the steady-state phase. This is supported by the increase of TWA NCE values up to 0.9968 while the time in this phase as well as normalised H_2 emissions decrease to 0.00005, as presented in Table 2. The gas-phase temperature profiles increase slightly with the PA, compared

to the natural draft case, except for the case of 118 L·min^{-1} in which the temperatures exceed all other measurements by approximately 150°C. This increase in temperature is related to the higher fuel conversion and the decrease of emissions of incomplete combustion, which will lead to a greater heat release in the system. Further addition of air leads to cooling due to air dilution.

As shown in Table 2, the TWA NCE values decrease from 0.9271 to 0.7773 in the char phase with higher PA flows. It is hypothesised that with a higher air flow the products of the gasification process, mainly CO, are not subsequently burned in flaming combustion on top of the fuel stack. The flames observed on top of the fuel stack in the gasification phase consume a higher proportion of the CO emissions in the natural draft case than with higher primary air flows. The higher flow rates appear to allow insufficient residence time for complete oxidation within the flaming region. This is supported by the gas-phase temperature profiles inside the combustor body. Temperatures increase with higher forced PA flow, but are consistently much lower than in the natural draft case. In addition, it can be assumed that the higher velocity of the migrating pyrolysis front, with higher PA flow, results in a higher initial heating rate of the solid fuel.[20] The initial heating rate has been shown to be decisive for the reactivity of the char.[42,43] Therefore, the high CO emissions especially at the beginning of the char phase could be caused by a higher reactivity of the remaining char after the steady-state phase.

3.3 Variation of Secondary Air

Figure 5 presents the normalised emissions and temperature profiles with varying secondary air as well as the natural draft case. It can be seen that in all phases the emissions are reduced substantially and the NCE is, except for the lowest value of SA, consistently higher than in the natural draft case. The initial peak of emissions in the lighting phase is reduced and the gas-phase temperatures inside the combustor body rise significantly.

In the steady-state phase it can be seen that the flow rate of 328 L·min^{-1} leads to

higher emissions than all the other cases, including the natural draft case. Thus, it can be assumed that a flow rate of 328 L·min^{-1} provides, as expected from the calculations presented in the Section 2.3.2, fuel-rich conditions and insufficient oxygen for complete combustion of the pyrolysis products. The NCE is consistently higher for all other air flows, compared to the natural draft case. In accordance, the gas-phase temperature inside the combustor extension is consistently higher. It should be highlighted that with the forced secondary air flows of 492 L·min^{-1} and 574 L·min^{-1} up to approximately 300°C higher temperatures can be measured.

In the char phase the reduction of emissions is especially significant, in relation to the natural draft case. The TWA NCE, as presented in Table 2, rises for all flow rates above 0.92 and up to 0.96 while the normalised H_2 value sinks as low as 0.00003. Values of such high efficiency had previously not been achieved in the char phase. This indicates that with higher secondary air flow rates a significantly greater proportion of CO emissions from the char gasification are oxidised. It should be stressed that only in the case of the two higher air flow rates the gas-phase temperatures inside the combustor body reach temperatures similar to the natural draft case. These high temperatures were only achieved with both airflows in natural draft configuration and with high SA flows, while temperatures with forced PA and natural draft SA were lower. Thus it can be assumed that the higher SA flow rates lead to a higher heat release from combustion in this phase.

A noticeable increase in efficiency is noted between the flow rates of 328 and 492 L·min^{-1}, but only a slight increase above that. This could mean that increasing the SA flow beyond a specified air to fuel ratio has only a marginal influence on the performance. It can be assumed that an optimal ratio of the PA to SA exists and that for a specific PA flow, lower SA flow values might lead to insufficient mixing of combustible gases with air, while an oversupply might lead to cooling and potentially quenching of the flame front. A ratio of PA to SA flow of about 1:4 appears to achieve a very high combustion efficiency for this configuration. Previously ratios of 1 to 3.1, 5.7, 6.2[28] and 2.3[44] have been reported,

but no relationship to the efficiency was established. Ratios of 1:3 and 1:4 have also been reported to achieve low CO emissions in the steady-state phase, where the char phase has not been considered.[31] Further investigation coupling the combustion efficiency with the heat transfer efficiency would be helpful in finding an optimal PA to SA flow ratio.

3.4 Variation of the Fuel Grate Location

The normalised emissions and temperature profiles of various fuel grate (FG) locations are presented in Figure 6. It can be seen that a reduction of the fuel stack distance to the SA inlet leads to higher measured temperatures inside the combustor extension ranging from 150°C to 250°C above the natural draft case. The increased temperature, compared to the natural draft case, of about 150°C with a FG distance of 470 mm can be attributed to the supply of forced primary air. The further temperature increase can be assumed to be due to the smaller distances of the FG. With a smaller distance between the fuel and the SA inlet there will be less heat loss of the gasification products before combustion, leading to an increase in the combustion temperature and thus efficiency. The higher temperatures will cause a greater buoyancy force at the SA inlet, increasing the amount of entering air, which in turn will effect the combustion efficiency. Decreasing emissions of products of incomplete combustion were recorded in the lighting and char phase, with smaller distances of the FG. Fuel grate locations of 180 and 270 mm provided NCE values of 0.9988 in the lighting phase, which were the highest of all measured configurations. A smaller distance of the fuel grate location also prolonged the high efficiency steady-state phase significantly, with a minor reduction of the NCE. In the char phase smaller distance of the FG caused a higher NCE, but only the lowest distance of 180 mm achieved a higher NCE than the natural draft configuration.

4 Discussion

Comparing the profiles, presented in Figures 4 and 5, it needs to be kept in mind that in the set of varying SA flow rates the PA was fixed to the value of 118 $L \cdot min^{-1}$ and the fuel grate location was at 470 mm below the SA inlet. Of special interest when relating these profiles to one another is that with higher SA flows the steady-state is longer and the emissions of incomplete combustion in the char phase are extensively mitigated, as can be seen in Table 2.

It has been established that the migrating pyrolysis is primarily governed by the PA flow.[12] Direct influence of the SA on the fuel stack is highly unlikely even at the highest air flows because of the large distance between the SA inlet and the fuel stack. This leads to the assertion that with a specified PA flow the migrating pyrolysis is of similar intensity and length. This raises the question how the introduction of forced SA prolongs the steady-state phase. From the temperature profiles and the NCE profiles in Figure 4 it can be deduced that the flame front at the SA inlet cannot be sustained at the end of the migrating pyrolysis, it extinguishes and subsequently high proportions of CO are emitted, in the configuration in which the SA is introduced by natural draft. In the forced SA cases, if the migrating pyrolysis is assumed to be of similar length as in the natural draft SA and 118 $L \cdot min^{-1}$ PA configuration, the flame does not extinguish at the end of this phase. With a flame present at the SA inlet the CO emissions which were emitted in the natural draft SA case are oxidised further. Therefore, it appears that with forced SA flow sufficient mixing of entering air and combustible gases, in conjunction with much higher temperatures in the combustor extension, can be achieved to sustain a flame at the SA inlet. With a flame present at the SA inlet a greater part of the CO emissions produced by the gasification process of char are burned in steady-state combustion, as can be seen in Figure 5. The combustion of CO from char gasification with increased secondary air at the secondary air inlet presents an extension of the steady-state combustion at this location, which was previously achieve only during the migrating pyrolysis.

A similar trend as with higher SA flows can be observed with smaller distances of the FG in the steady-state phase. The steady-state phase lasts much longer, for 419 s, with the lowest distance of the FG, compared to 179 s with the greatest distance. Similar to the forced SA air cases much higher gas-phase temperatures were also measured in the combustor extension. In Figure 6 it can be seen that the measured gas temperature inside the combustor extension is approximately 100°C higher with a FG distance of 180 mm compared with 470 mm. When the gas temperature is higher there is an increase in buoyancy-induced flow due to the greater density difference between the gases inside the combustor extension and the cold secondary air. Accordingly, the higher air flow, with smaller distance of the FG, in conjunction with the higher temperatures appear to keep a flame present at the SA inlet during the combustion of gasification products from mainly raw biomass and into the combustion of mainly CO from char gasification. This extension of the steady-state combustion, to include combustion of char gasification products, seems to be the reason for a longer duration of this phase and a reduction of overall CO emissions.

In the char phase the reduction of emissions, especially CO, with the higher SA flow, is a result of a combination of the longer steady-state phase and the influence of the SA on the air flow inside the combustor body. A higher efficiency and the combustion of char gasification products at the end of the steady-state phase, will lead to a much lower amount of char remaining after this phase. The lower amount of remaining char alone cannot explain the much higher NCE in the char phase with increasing SA flow. Therefore, the SA must also have an influence on the flow field inside the combustor body. The increasing amount of forced SA being introduced will lead to better mixing and more complete combustion in the secondary flame front. Future studies of the influence of SA on the flow field inside staged combustors could provide deeper insights.

The direct application of the current findings in cookstoves is primarily limited by the chosen research approach, which is focussed specifically on the combustion science of the

thermochemical process. In this study measurements were carried out without emulating user practice or performing cooking tasks. Therefore, the influence of a cooking pot on top of the stove on the combustion performance is unknown. Similarly, with a smaller diameter reactor the influence of quenching by the cold walls may become more pronounced. In an optimised system, it is aspirational for combustion to be completed before contact with the cooking surface or walls. The heat transfer to the pot would then be exclusively achieved by hot flue gases. Hence, in such a system the combustion properties would be independent of the cooking performance. To achieve such a system, further fundamental research on the gasification and combustion behaviour of staged combustors, using different fuels and air supply conditions as well as the heat transfer properties would be beneficial.

5 Conclusions

The present study investigates the influence of the primary and secondary air, with natural draft as well as forced draft, in various relations to each other, on the combustion process in a staged combustor. The location of fuel within the combustor was modified to simulate the variation of the relative position of the primary and secondary air inlet to the fuel stack. This study presents general insights into the combustion processes in small-scale staged combustion devices. The combustor used for this research was custom made for the purpose of studying the ongoing combustion processes and is not being used for cooking, which limits the comparability to commercial products which are usually tested while performing certain cooking tasks.

In the lighting phase, emissions of incomplete combustion can be significantly reduced by providing a sufficient air supply. This can be achieved by either ensuring that the top of the fuel stack is always as close as possible to the secondary air (SA) inlet, which achieves highest efficiency, or by introducing SA by forced draft. When using forced draft the peak

NCE rises by increasing the primary air (PA) air flow, from 0.84 with natural draft up to 0.96, but even more so by increasing the SA flow, up to 0.99.

The migrating pyrolysis is governed by the PA flow with higher flows increasing the heat release. During the migrating pyrolysis the products are oxidised in steady-state combustion at the secondary air inlet. When using a combination of forced PA supply and natural draft SA, an increase of PA leads to a shorter time in this steady-state phase with higher combustion temperatures and a higher NCE. Introducing forced SA in combination with forced PA leads to longer steady-state combustion, extending it from primarily combustion of volatile pyrolysis products to combustion of primarily carbon monoxide from char gasification. This provides a drastic reduction of products of incomplete combustion and a significant increase in efficiency. A considerable increase in combustion efficiency was identified for PA to SA flow ratios of up to 1:4, for the wood chips fuel. Reducing the distance between the SA inlet and the fuel stack, with SA introduced by natural draft, had a similar effect to increasing the SA via forced draft. Therefore, an adjustable fuel grate, to be able to use a variable amount fuel without increasing the release of emissions of incomplete combustion, should be considered for any staged combustor design. Future work including the influence of the fuel stack depth on the combustion process would be beneficial.

In the char phase, increasing the PA flow produced significantly more emissions of incomplete combustion. With the addition of an increased amount of forced SA these emissions could be burned cleanly.

In the present study different air requirements for the three phases lighting, steady-state and char, have been identified. The application of dynamic air control, rather than a constant air supply, to suit each phase could be the topic of future research. Furthermore, it could be shown that forced PA in combination with natural draft SA is not a beneficial option. To achieve low emissions in this configuration it would require attentive handling to reduce the PA flow after the steady-state phase. Forced draft for the PA as well as SA

flow to increases the controllability and efficiency in all phases. To achieve low emissions of incomplete combustion, fuel-lean conditions must be ensured in the secondary flame front. The combustion efficiency is also greater with a smaller distance between the fuel and the SA inlet.

6 Acknowledgements

The authors wish to acknowledge the support of The University of Adelaide and Marc Simpson, the laboratory facilities manager. The contributions to the provision and analysis of the experiments by Aleksis Xenophon, James Metcalfe and Oliver Robson are greatly appreciated. Thomas Kirch gratefully acknowledges the support provided by the Studienstiftung des Deutschen Volkes.

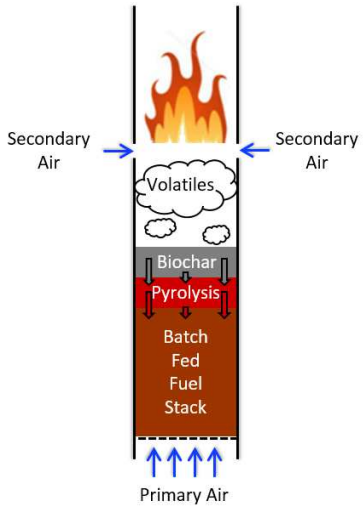

Figure 1: Schematic illustration of the combustion process in a staged combustor.

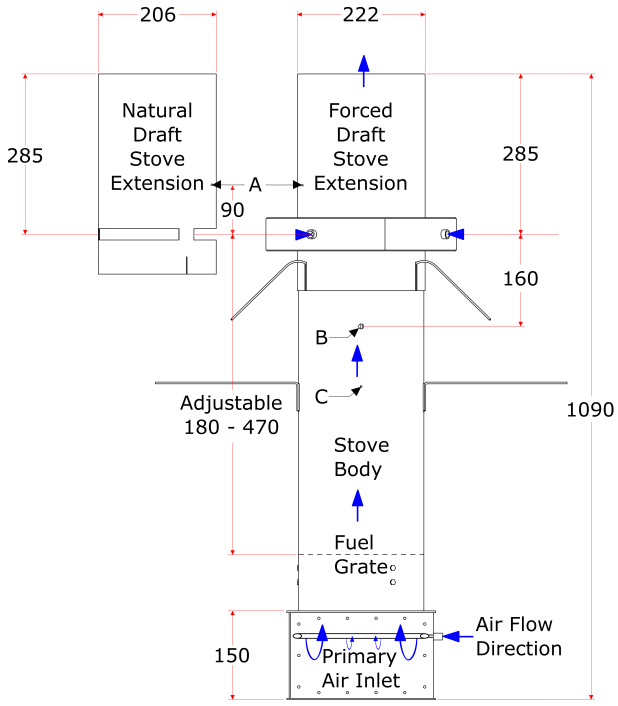

Figure 2: Schematic diagram of the combustor, with inlet locations for thermocouples (A, B) and measuring location of the outer combustor body temperature (C), with the air flow direction and all numeric values in millimetres.

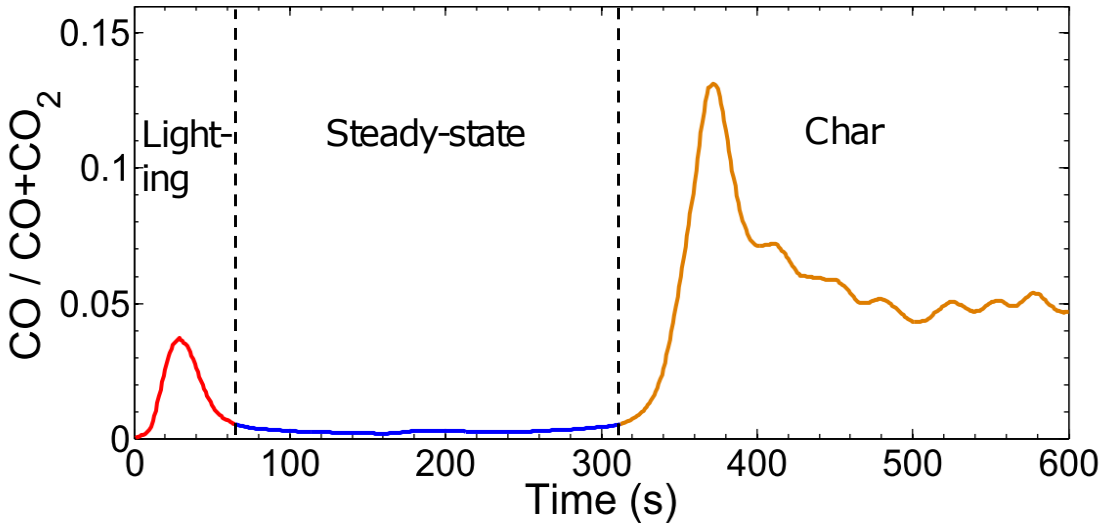

Figure 3: Normalised CO emissions profile with separated phases by the mathematical decision rule. Phase change was identified when the temporal derivative of the normalised CO profile ($X_{CO}/(X_{CO}+X_{CO_2})$) exceeded a value of $\pm 0.002\ s^{-1}$.

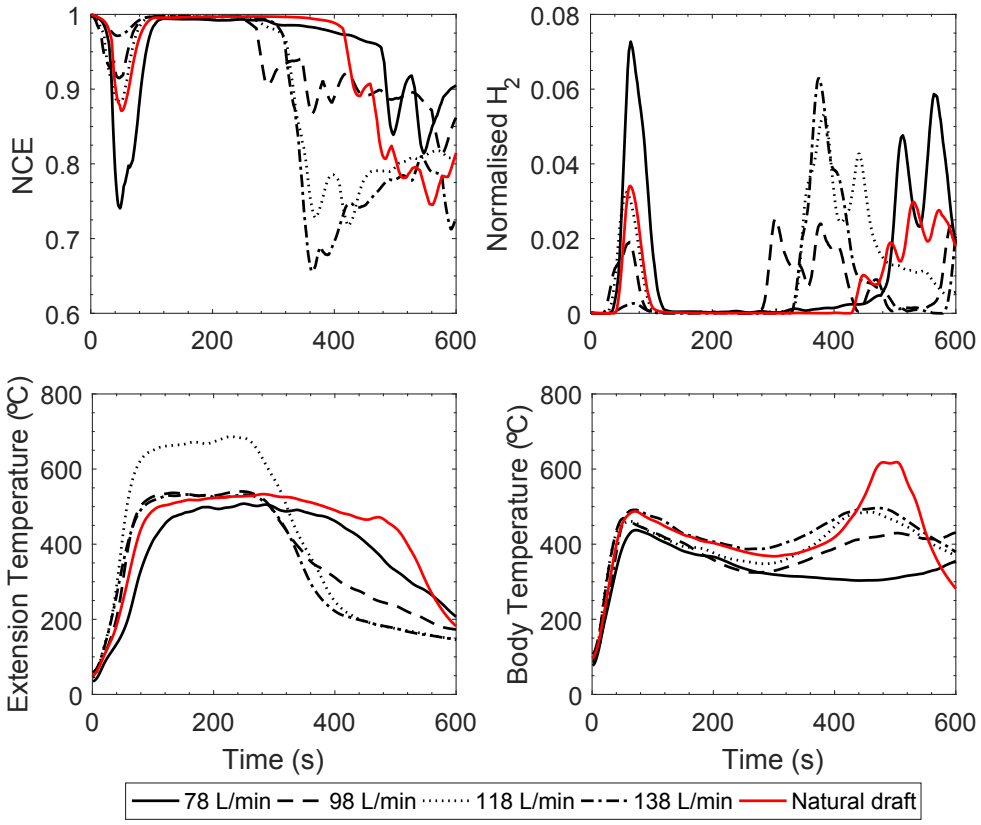

Figure 4: Average normalised emissions profiles of H_2, the nominal combustion efficiency (NCE = $X_{CO_2}/(X_{CO}+X_{CO_2})$) and measured gas-phase temperature profiles, inside the combustor body and the combustor extension, for various primary air flows, and the natural draft case.

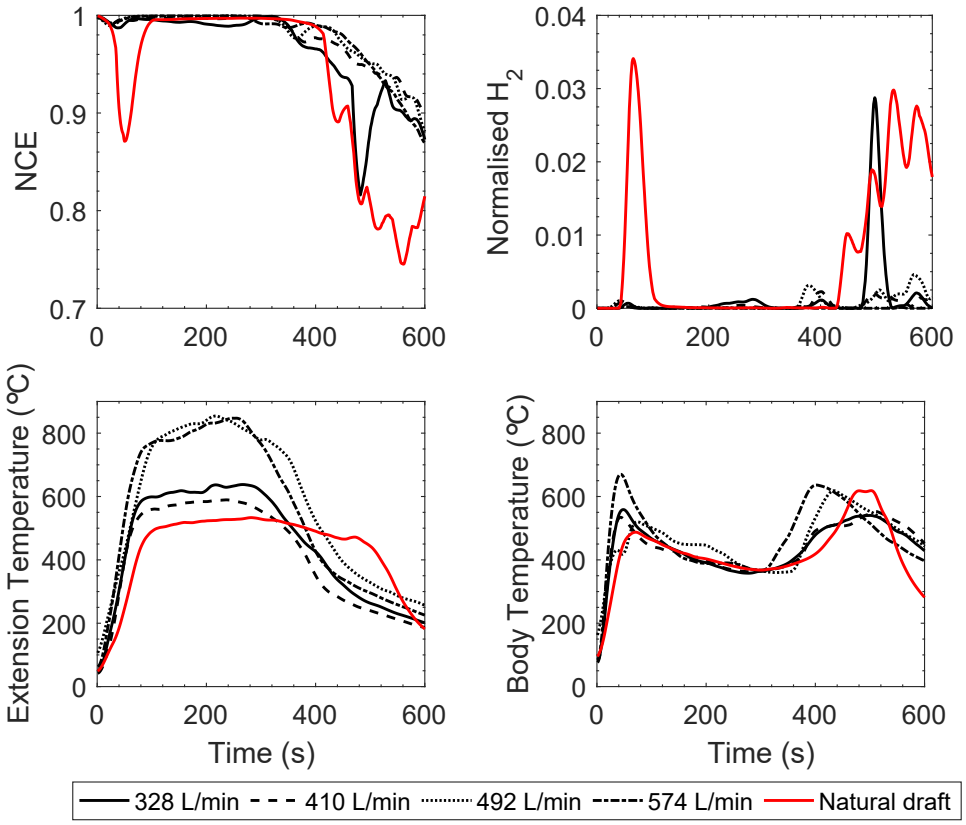

Figure 5: Average normalised emissions profiles of H_2, the nominal combustion efficiency (NCE = $X_{CO_2}/(X_{CO}+X_{CO_2})$) and measured gas-phase temperature profiles, inside the combustor body and the combustor extension, for various secondary air flows, at 118 L·min^{-1} primary air flow, and the natural draft case.

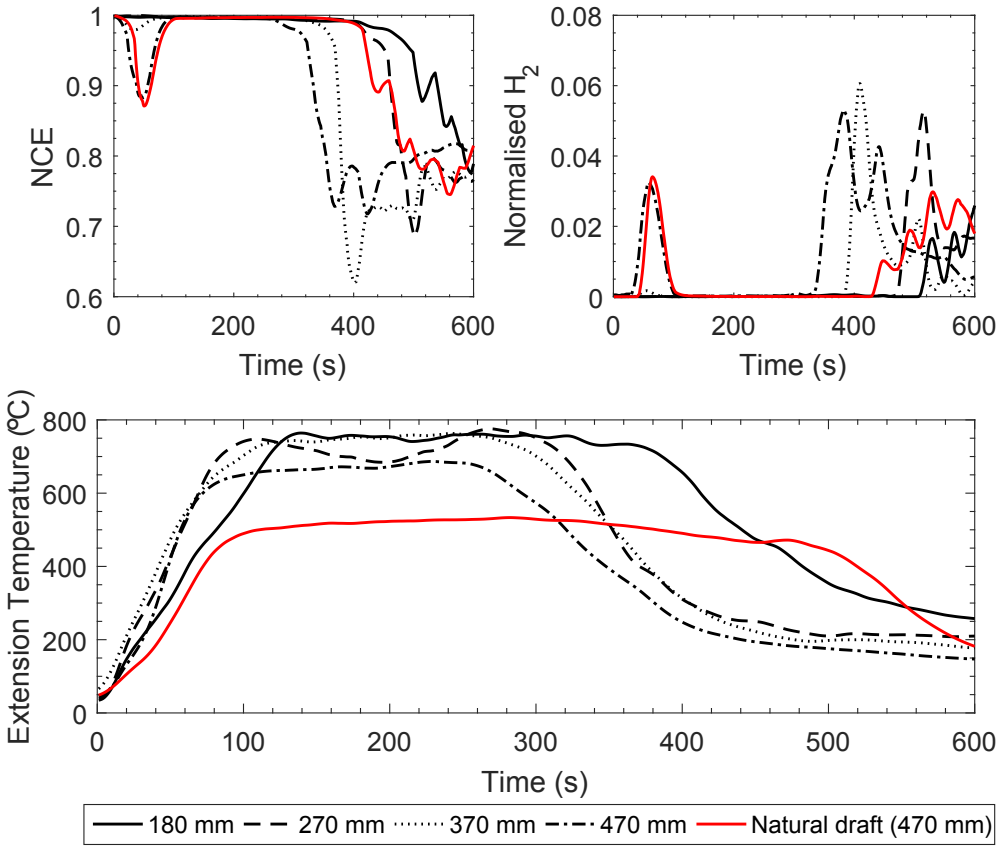

Figure 6: Average normalised emissions profiles of H_2, the nominal combustion efficiency (NCE = $X_{CO_2}/(X_{CO}+X_{CO_2})$) and measured gas-phase temperature profiles, inside the combustor extension, for varying distances of the fuel grate below the SA inlet, at 118 L·min^{-1} primary air flow, and the natural draft case.

Table 1: Configurations of the natural draft (ND), varying primary air (PA), varying secondary air (SA) and varying fuel grate locations (FGL) below the SA inlet cases that were tested.

	Repetitions	PA flow[L min^{-1}]	SA flow[L min^{-1}]	FGL [mm]	Equivalence Ratio (Φ)
Both Natural draft	8	ND	ND	470	
Varying primary air	5	78	ND	470	
	4	98	ND	470	
	6	118	ND	470	
	6	138	ND	470	
Varying secondary air	4	118	328	470	1.11
	3	118	410	470	0.94
	3	118	492	470	0.81
	3	118	574	470	0.71
Varying fuel grate location	4	118	ND	180	
	3	118	ND	270	
	3	118	ND	370	
	6	118	ND	470	

Table 2: Average peak emissions in the lighting phase and time weight average (TWA) emissions in the steady-state and the char phase for all four investigated cases, with the standard deviation in parenthesis.

	Natural draft	**Varying primary air [L·min^{-1}]**				**Varying secondary air [L·min^{-1}]**				**Varying fuel grate location [mm]**			
		78	**98**	**118**	**138**	**328**	**410**	**492**	**574**	**180**	**270**	**370**	**470**
	Lighting phase					**Lighting phase**				**Lighting phase**			
Min NCE	0.8404 (0.1659)	0.6155 (0.1424)	0.8639 (0.1233)	0.8266 (0.1597)	0.9631 (0.0124)	0.9851 (0.0045)	0.9868 (0.0004)	0.9889 (0.0012)	0.9920 (0.0019)	0.9988 (0.0005)	0.9988 (0.0011)	0.9785 (0.0029)	0.8267 (0.1597)
Max H2 Peak	0.0418 (0.0538)	0.1044 (0.0513)	0.0314 (0.0352)	0.0447 (0.0466)	0.0043 (0.0027)	0.0007 (0.0007)	0.001 (0.0005)	0.00105 (0.0009)	0.00023 (0.0004)	0.0 (0.00000)	0.00047 (0.00082)	0.00179 (0.00057)	0.0447 (0.04656)
	Steady-state phase					**Steady-state phase**				**Steady-state phase**			
Time in Phase	285.4 (27.7)	281.4 (121.3)	224.5 (67.7)	178.8 (19.8)	213.7 (21.6)	275.7 (20.6)	263.0 (30.2)	279.3 (15.0)	242.7 (29.5)	419.25 (29.3)	398.0 (25.0)	258.3 (17.0)	178.8 (19.7)
TWA - NCE	0.9965 (0.0006)	0.9931 (0.0024)	0.9963 (0.0008)	0.9970 (0.0007)	0.9968 (0.0008)	0.9938 (0.0016)	0.9977 (0.0018)	0.9989 (0.0004)	0.9991 (0.0003)	0.9951 (0.0016)	0.9966 (0.0002)	0.9970 (0.0004)	0.9970 (0.0007)
TWA - H2	0.00013 (0.00015)	0.00049 (0.0004)	0.00021 (0.00017)	0.0003 (0.00024)	0.00005 (0.00005)	0.0003 (0.00008)	0.00013 (0.00021)	0.00006 (0.00006)	0.00001 (0.00001)	0.00013 (0.00014)	0.00020 (0.0002)	0.00002 (0.00001)	0.0003 (0.00024)
	Char phase					**Char phase**				**Char phase**			
TWA - NCE	0.8518 (0.0428)	0.9271 (0.0348)	0.8912 (0.0532)	0.8303 (0.0182)	0.7773 (0.0225)	0.9277 (0.0356)	0.9549 (0.0165)	0.9590 (0.0156)	0.9600 (0.0026)	0.9089 (0.0105)	0.8340 (0.0084)	0.7788 (0.0156)	0.8303 (0.0182)
TWA - H2	0.01368 (0.00727)	0.01667 (0.01008)	0.01026 (0.00286)	0.01679 (0.00516)	0.01343 (0.00396)	0.00277 (0.00384)	0.00078 (0.00073)	0.00135 (0.00145)	0.00003 (0.00003)	0.00645 (0.00284)	0.01536 (0.00397)	0.01207 (0.00174)	0.01679 (0.00516)

7 References

References

(1) Bonjour, S.; Adair-Rohani, H.; Wolf, J.; Bruce, N. G.; Mehta, S.; Prüss-Ustün, A.; Lahiff, M.; Rehfuess, E. A.; Mishra, V.; Smith, K. R. Solid fuel use for household cooking: Country and regional estimates for 1980-2010. *Environmental Health Perspectives* **2013**, *121*, 784–790.

(2) Lelieveld, J.; Evans, J. S.; Fnais, M.; Giannadaki, D.; Pozzer, a. The contribution of outdoor air pollution sources to premature mortality on a global scale. *Nature* **2015**, *525*, 367–71.

(3) Murray, C. J. L.; Forouzanfar, M. H.; Alexander, L.; Anderson, H. R.; Bachman, V. F. Global, regional and national comparative risk assessment of 79 behavioural, environmental/occupational and metabolic risks or clusters of risks in 188 countries 1990-2013: a systematic analysis for the Global Burden of Disease Study 2013. *Lancet in print* **2015**, *6736*, 1998–2005.

(4) Sovacool, B. K. The political economy of energy poverty: A review of key challenges. *Energy for Sustainable Development* **2012**, *16*, 272–282.

(5) Anenberg, S. C.; Balakrishnan, K.; Jetter, J.; Masera, O.; Mehta, S.; Moss, J.; Ramanathan, V. Cleaner cooking solutions to achieve health, climate, and economic cobenefits. *Environmental Science and Technology* **2013**, *47*, 3944–3952.

(6) Jetter, J.; Zhao, Y.; Smith, K. R.; Khan, B.; Yelverton, T.; DeCarlo, P.; Hays, M. D. Pollutant emissions and energy efficiency under controlled conditions for household biomass cookstoves and implications for metrics useful in setting international test standards. *Environmental Science and Technology* **2012**, *46*, 10827–10834.

(7) Jetter, J. J.; Kariher, P. Solid-fuel household cook stoves: Characterization of performance and emissions. *Biomass and Bioenergy* **2009**, *33*, 294–305.

(8) Houshfar, E.; Skreiberg, Ø.; Løvås, T.; Todorović, D.; Sørum, L. Effect of excess air ratio and temperature on NOx emission from grate combustion of biomass in the staged air combustion scenario. *Energy and Fuels* **2011**, *25*, 4643–4654.

(9) Reed, T. B.; Larson, R. A wood-gas stove for developing countries. *Energy for Sustainable Development* **1996**, *3*, 34–37.

(10) Arora, P.; Das, P.; Jain, S.; Kishore, V. V. N. A laboratory based comparative study of Indian biomass cookstove testing protocol and Water Boiling Test. *Energy for Sustainable Development* **2014**, *21*, 81–88.

(11) Roth, C. Micro-gasification : cooking with gas from dry biomass. GIZ - Deutsche Gesellschaft fuer Internationale Zusammenarbeit, 2014; `http://www.giz.de/fachexpertise/downloads/giz2014-en-micro-gasification-manual-hera.pdf`.

(12) Reed, T.; Walt, R.; Ellis, S.; Das, A.; Deutch, S. Superficial Velocity - The Key To Downdraft Gasification. 4th Biomass Conference of the Americas. Oakland, California, 1999; pp 1–8.

(13) Yibo, H.; Li, H.; Chen, X.; Xue, C.; Chen, C.; Liu, G. Effects of moisture content in fuel on thermal performance and emission of biomass semi-gasified cookstove. *Energy for Sustainable Development* **2014**, *21*, 60–65.

(14) Branca, C.; Di Blasi, C. Global Kinetics of Wood Char Devolatilization and Combustion. *Energy and Fuels* **2003**, *17*, 1609–1615.

(15) Birzer, C.; Medwell, P.; MacFarlane, G.; Read, M.; Wilkey, J.; Higgins, M.; West, T. A Biochar-producing, Dung-burning Cookstove for Humanitarian Purposes. *Procedia Engineering* **2014**, *78*, 243–249.

(16) Fatehi, M.; Kaviany, M. Adiabatic reverse combustion in a packed bed. *Combustion and Flame* **1994**, *99*, 1–17.

(17) Rönnbäck, M.; Axell, M.; Gustavsson, L.; Thunman, H.; Lecher, B. In *Progress in Thermochemical Biomass Conversion*; Bridgwater, A., Ed.; Blackwell Science Ltd: Bodmin, 2001; Chapter 59, pp 743–757.

(18) Horttanainen, M.; Saastamoinen, J.; Sarkomaa, P. Operational limits of ignition front propagation against airflow in packed beds of different wood fuels. *Energy and Fuels* **2002**, *16*, 676–686.

(19) Yang, Y. B.; Sharifi, V. N.; Swithenbank, J. Effect of air flow rate and fuel moisture on the burning behaviours of biomass and simulated municipal solid wastes in packed beds. *Fuel* **2004**, *83*, 1553–1562.

(20) Porteiro, J.; Patiño, D.; Collazo, J.; Granada, E.; Moran, J.; Miguez, J. L. Experimental analysis of the ignition front propagation of several biomass fuels in a fixed-bed combustor. *Fuel* **2010**, *89*, 26–35.

(21) Porteiro, J.; Patiño, D.; Moran, J.; Granada, E. Study of a fixed-bed biomass combustor: Influential parameters on ignition front propagation using parametric analysis. *Energy and Fuels* **2010**, *24*, 3890–3897.

(22) Buchmayr, M.; Gruber, J.; Hargassner, M.; Hochenauer, C. Experimental investigation of the primary combustion zone during staged combustion of wood-chips in a commercial small-scale boiler. *Biomass and Bioenergy* **2015**, *81*, 356–363.

(23) Kuo, J. T.; Hsu, W.-S.; Yo, T.-C. Effect of Air Distribution on Solid Fuel Bed Combustion. *Journal of Energy Resources Technology* **1997**, *119*, 120.

(24) MacCarty, N.; Still, D.; Ogle, D. Fuel use and emissions performance of fifty cooking

stoves in the laboratory and related benchmarks of performance. *Energy for Sustainable Development* **2010**, *14*, 161–171.

(25) Aprovecho Research Center, Test Results of Cook Stove Performance. 2011; `http://aprovecho.org/publications-3/`.

(26) Kumar, M.; Kumar, S.; Tyagi, S. Design, development and technological advancement in the biomass cookstoves: A review. *Renewable and Sustainable Energy Reviews* **2013**, *26*, 265–285.

(27) Kshirsagar, M. P.; Kalamkar, V. R. A comprehensive review on biomass cookstoves and a systematic approach for modern cookstove design. *Renewable and Sustainable Energy Reviews* **2014**, *30*, 580–603.

(28) Reed, T. B.; Anselmo, E.; Kircher, K. In *Progresss in Thermochemical Biomass Conversion Conference*; Bridgwater, A., Ed.; Blackwell Science Ltd: Bodmin, 2001; pp 693 – 704.

(29) Mukunda, H. S.; Dasappa, S.; Paul, P. J.; Rajan, N. K. S.; Yagnaraman, M.; Ravi Kumar, D.; Deogaonkar, M. Gasifier stoves - science, technology and field outreach. *Current Science* **2010**, *98*, 627–638.

(30) Varunkumar, S.; Rajan, N. K. S.; Mukunda, H. S. Experimental and computational studies on a gasifier based stove. *Energy Conversion and Management* **2012**, *53*, 135–141.

(31) Tryner, J.; Tillotson, J. W.; Baumgardner, M. E.; Mohr, J. T.; Defoort, M. W.; Marchese, A. J. The effects of fuel properties , air flow rates , secondary air inlet geometry , and operating mode on the performance of TLUD semi-gasifier cookstoves. *Environmental Science and Technology* **2016**,

(32) Kirch, T.; Medwell, P. R.; Birzer, C. H. Natural draft and forced primary air combus-

tion properties of a top-lit up-draft research furnace. *Biomass and Bioenergy* **2016**, *91*, 108–115.

(33) Eskilsson, D.; Rönnbäck, M.; Samuelsson, J.; Tullin, C. Optimisation of efficiency and emissions in pellet burners. *Biomass and Bioenergy* **2004**, *27*, 541–546.

(34) Carroll, J. P.; Finnan, J. M.; Biedermann, F.; Brunner, T.; Obernberger, I. Air staging to reduce emissions from energy crop combustion in small scale applications. *Fuel* **2015**, *155*, 37–43.

(35) Lombardi, F.; Riva, F.; Bonamini, G.; Barbieri, J. Laboratory protocols for testing of Improved Cooking Stoves (ICSs): A review of state-of-the-art and further developments. *Biomass and Bioenergy* **2017**, *98*, 321–335.

(36) Birzer, C.; Medwell, P.; Wilkey, J.; West, T.; Higgins, M.; Macfarlane, G.; Read, M. An analysis of combustion from a top-lit up-draft (TLUD) cookstove. *Journal of Humanitarian Engineering* **2013**, *2*, 1–8.

(37) Kirch, T.; Medwell, P. R.; Birzer, C.; Holden, L. The role fo primary and secondary air on wood combustion in cookstoves. *International Journal of Sustainable Energy* **2016**,

(38) Yevich, R.; Logan, J. A. An assessment of biofuel use and burning of agricultural waste in the developing world. *Global Biogeochemical Cycles* **2003**, *17*.

(39) American Society for Testing and Materials, ASTM D4442-92(2003): Standard Test Methods for Direct Moisture Content Measurement of Wood and Wood-based Materials. 2003.

(40) Johnson, M.; Edwards, R.; Berrueta, V.; Masera, O. New approaches to performance testing of improved cookstoves. *Environmental Science and Technology* **2010**, *44*, 368–374.

(41) Kirch, T.; Medwell, P. R.; Birzer, C. H. Assessment of natural draft combustion properties of top-lit up-draft research furnace. Australian Combustion Symposium 2015 Proceedings. Melbourne, 2015.

(42) Janse, A. M. C.; Jonge, H. G. D.; Prins, W.; Swaaij, W. P. M. V. Combustion Kinetics of Char Obtained by Flash Pyrolysis of Pine Wood. *Ind. Eng. Chem. Res.* **1998**, *37*, 3909–3918.

(43) Dall'Ora, M.; Jensen, P. A.; Jensen, A. D. Suspension combustion of wood: Influence of pyrolysis conditions on char yield, morphology, and reactivity. *Energy and Fuels* **2008**, *22*, 2955–2962.

(44) Raman, P.; Ram, N. K.; Gupta, R. Development, design and performance analysis of a forced draft clean combustion cookstove powered by a thermo electric generator with multi-utility options. *Energy* **2014**, *69*, 813–825.